How to cite: *Angew. Chem. Int. Ed.* **2023**, *62*, e202308004
doi.org/10.1002/anie.202308004

Molecular Glues | Hot Paper

From Tethered to Freestanding Stabilizers of 14-3-3 Protein-Protein Interactions through Fragment Linking

Emira J. Visser[+], Priyadarshini Jaishankar[+], Eline Sijbesma[+], Marloes A. M. Pennings, Edmee M. F. Vandenboorn, Xavier Guillory, R. Jeffrey Neitz, John Morrow, Shubhankar Dutta, Adam R. Renslo, Luc Brunsveld,* Michelle R. Arkin,* and Christian Ottmann**

Abstract: Small-molecule stabilization of protein-protein interactions (PPIs) is a promising strategy in chemical biology and drug discovery. However, the systematic discovery of PPI stabilizers remains a largely unmet challenge. Herein we report a fragment-linking approach targeting the interface of 14-3-3 and a peptide derived from the estrogen receptor alpha (ERα) protein. Two classes of fragments—a covalent and a noncovalent fragment—were co-crystallized and subsequently linked, resulting in a noncovalent hybrid molecule in which the original fragment interactions were largely conserved. Supported by 20 crystal structures, this initial hybrid molecule was further optimized, resulting in selective, 25-fold stabilization of the 14-3-3/ERα interaction. The high-resolution structures of both the single fragments, their co-crystal structures and those of the linked fragments document a feasible strategy to develop orthosteric PPI stabilizers by linking to an initial tethered fragment.

[*] E. J. Visser,[+] E. Sijbesma,[+] M. A. M. Pennings, E. M. F. Vandenboorn, X. Guillory, L. Brunsveld, C. Ottmann
Laboratory of Chemical Biology, Department of Biomedical Engineering and Institute for Complex Molecular Systems (ICMS), Eindhoven University of Technology
Den Dolech 2, 5612 AZ Eindhoven (The Netherlands)
E-mail: l.brunsveld@tue.nl
c.ottmann@tue.nl

P. Jaishankar,[+] R. J. Neitz, J. Morrow, S. Dutta, A. R. Renslo, M. R. Arkin
Department of Pharmaceutical Chemistry and Small Molecule Discovery Centre (SMDC), University of California San Francisco (UCSF)
San Francisco, CA 94143 (USA)
E-mail: adam.renslo@ucsf.edu
michelle.arkin@ucsf.edu

[+] These authors contributed equally to this work.

Introduction

Pharmacological intervention of PPIs is undoubtedly a very attractive approach to modulate protein function. Whereas both convincing success stories and proven strategies exist for developing PPI inhibitors, conceptually validated approaches for targeted and specific stabilization of PPIs are scarce. However, adding to the initial description of natural product therapeutics such as rapamycin and FK506 as "molecular glues",[1] the tremendous success of PROTACs (proteolysis targeting chimeras), IMiDs (immunomodulatory drugs) and "molecular glue degraders" have sparked significant interest in the "three-body-challenge" of small-molecule PPI stabilization.[1–3] While there are examples of bioactive small molecules that act by stabilizing PPIs, in the majority of cases their discovery was due to serendipity rather than prospective mechanistic insight.[4]

One protein class attractive for PPI stabilization is the 14-3-3 family of phosphoserine/threonine-recognizing adapter proteins. These proteins interact with several hundred partner proteins[5] and modulate the activity of disease-driving proteins e.g., Raf kinases,[6–8] p53[9–12] (cancer), Tau[13–15] (Alzheimer's), LRRK2[16,17] (Parkinson's), NFκB[18,19] (inflammation), and ExoS[20,21] (infection). Not surprisingly, molecules able to modulate these interactions have been of significant interest for chemical biology and increasingly as guiding principles for potential therapeutic intervention.[22,23] In addition to natural products,[24–26] supramolecular ligands,[27] and more "conventional" molecules,[28,29] our groups have recently proposed fragments as starting points for the development of 14-3-3 PPI stabilizers.[30–33]

Fragment-based drug discovery (FBDD) is a widely applied technology to find ligand-efficient chemical matter in drug discovery projects. In FBDD, molecules with a molecular weight below 200 Da, which typically bind with low affinities in the mM range, are identified by sensitive biophysical techniques like NMR, SPR-, and X-ray crystallography. Approved drugs like the B-RAF inhibitor vemurafenib[34] and Bcl-2 inhibitor venetoclax[35] have been developed using FBDD. Although one of the promises of fragment-based development was to link neighboring fragments,[36] successful use of the strategy has been described in only a few cases.[37,38] Two challenges that confound fragment linking are identifying linker chemistry

that conserves the binding orientations of both fragments and the lack of suitable neighboring pockets in many protein targets.[36,39] Consequently, the vast majority of fragment optimization is achieved by "fragment-growing" rather than "fragment-linking".[40,41] Nonetheless, when fragment linking has worked, high affinity was rapidly achieved.[36,42,43]

In two previous screening campaigns, we identified fragments that bound near the interface of the adapter protein 14-3-3 with a phosphopeptide derived from the C-termini of the transcription factors ERα (estrogen receptor alpha) and p53. One class of fragments (**class I**) were covalent molecules identified by "tethering", which employed an engineered cysteine in 14-3-3 near the ERα phosphopeptide binding site[30] (Figure 1a). These fragments stabilized the 14-3-3/ERα complex up to 40-fold by engaging the C-terminal residue of ERα, Val595. The second group of fragments (**class II**), identified by soaking of 14-3-3/p53 crystals with fragment cocktails, bound to 14-3-3 further from the peptide binding site[33] (Figure 1b). Herein, we demonstrate an approach for linking a tethered and a noncovalent fragment using constraints defined by co-crystallography (Figure 1c). The resulting noncovalent molecules stabilized the 14-3-3γ/ERα-phosphopeptide complex efficiently and selectively. Such compounds are promising starting points for medicinal chemistry optimization, and are among[44] the first examples of molecular glues discovered by fragment linking. This work also represents a rare example of covalent fragments yielding reversible, noncovalent leads for a PPI.

Results and Discussion

The first class of fragments, exemplified by compound **1**, was "tethered" through an engineered cysteine at position 42 in the 14-3-3 protein and extended a halogenated benzyl ring (chlorophenyl) into a deep composite pocket formed between 14-3-3 and the C-terminal valine of the ERα phosphopeptide (Figure 1a, d). The other class of frag-

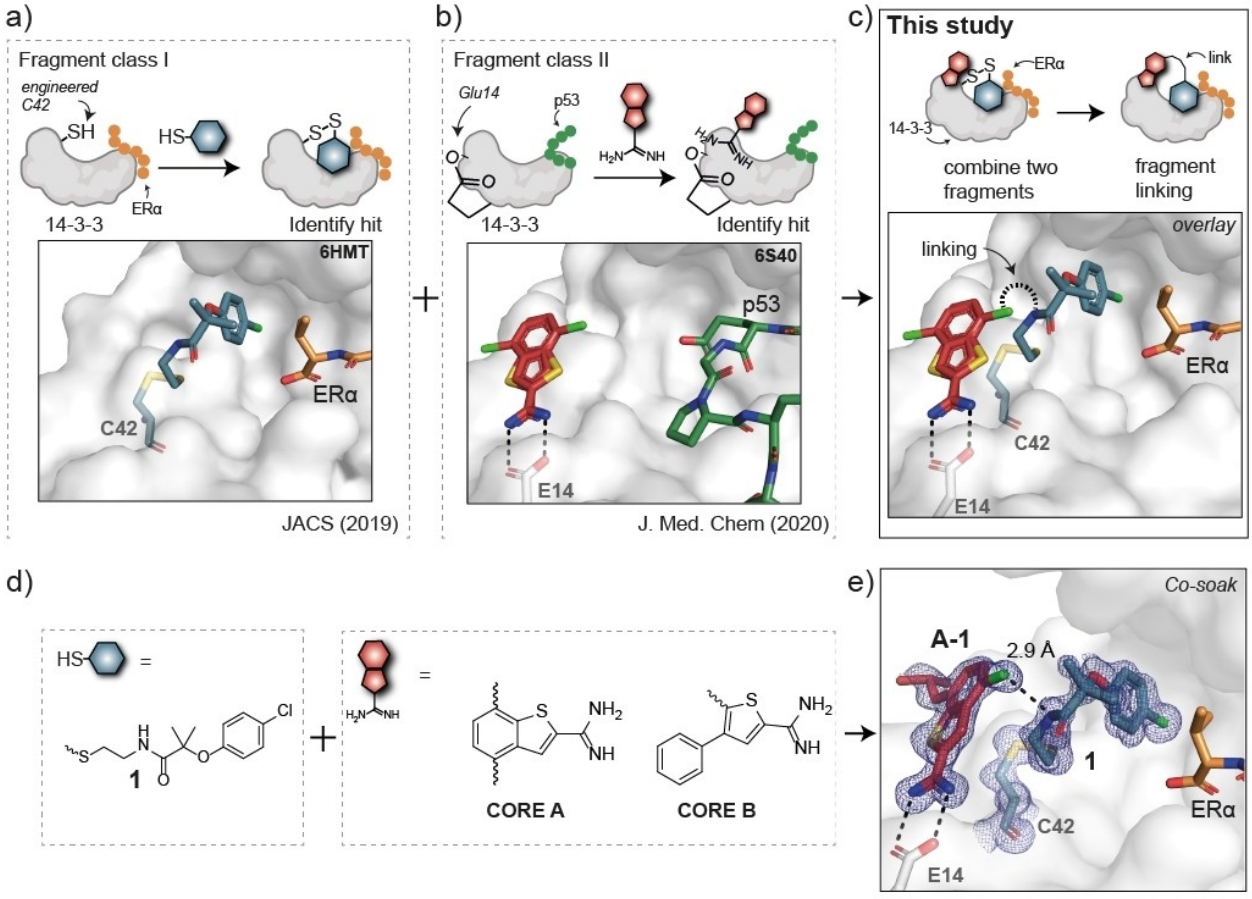

Figure 1. Overview of fragment linking approach. a) Schematic and X-ray crystal structure of previously discovered C42 tethered fragment **1** (blue sticks) in complex with 14-3-3σ (N42 C, C38 A; white surface) and ERα phosphopeptide (orange sticks) (pdb ID: 6HMT). b) Schematic illustration and X-ray crystal structure of previously discovered amidine fragment (red sticks) in complex with 14-3-3σ (white surface) and p53 phosphopeptide (green sticks; pdb ID: 6S40). c) Schematic illustration of fragment linking approach taken in this study and crystallographic overlay of the two previously discovered fragments to show their proximity. d) Structures of two fragment classes with disulfide tethered fragment **1** and benzothiophene **Core A** and phenylthiophene **Core B**. e) X-ray crystal structure of co-soak of compound **1** (blue sticks) and **A-1** (red sticks) in complex with 14-3-3σ (white surface) and ERα phosphopeptide (orange sticks). 2Fo–Fc electron density map is contoured at 1σ.

ments consisted of a benzo[*b*]thiophene-2-carboximidamide (**Core A**) or a 4-phenylthiophene-2-carboximidamide (**Core B**; Figure 1b, d and Figure S1). Soaking the thiophene-containing fragments (**A-1**–**A-3** and **B-1**–**B-3**) into 14-3-3/ERα co-crystals revealed engagement of their amidine functional group with Glu14 of 14-3-3 through a salt bridge, defining the primary anchoring point of these fragments[33] (Figure S2). To determine if fragments bound compatibly with compound **1**, 14-3-3/ERα crystals were soaked with compound **1** and the class II fragments. Comparison of the single benzothiophene soaks with their compound **1** co-soaks revealed a slight tilt of the benzo[*b*]thiophene fragments to prevent a steric clash, while the conformation of compound **1** remained unchanged (Figure S3a–c). In this slightly altered conformation, the binding sites of the two fragment groups lay next to each other, within a distance of 3 to 4 Å (Figure 1e, Figure S3d–f).

Based on the structural information of the co-soaks, we designed four benzothiophene-containing linked fragments with varying linker length and rigidity (compounds **2**–**5**), aiming to retain key binding contacts, including the amidine-mediated binding to Glu14 of 14-3-3 and the positioning of the *p*-chlorophenyl ring towards the C-terminal valine of ERα (Figure 2a). Only compound **5** showed partial electron density for both the benzothiophene and *p*-chlorophenyl rings of the hybrid molecule (Figure 2b). Overlaying its structure with those of single and co-soaks of the benzothiophene cores (Figure S4) revealed that the orientation of the benzothiophene in the hybrid molecule was spatially between its orientation in single and co-soaked structures. The *p*-chlorophenyl ring of **5** also adopted a different conformation than compound **1** (Figure 2c). The slightly different positions of the linked fragments as compared to that in their individual soaks suggested a non-ideal linker, perhaps explaining the lack of density in this region of the complex structure of **5**.

Next, we designed and synthesized three linked fragments (compounds **6**–**8**) containing the phenylthiophene moiety (Figure 2d). Excitingly, continuous electron density was visible for amidine **6** (Figure 2e), which also showed modest stabilization of 14-3-3/ERα in the high μM to mM range (Figure S5a). Of note, neither the amidoxime **7** nor carboxamide analogue **8** were active (Figure S5a). A crystallographic overlay of the hybrid molecule **6** with the single phenylthiophene soaks (Figure S5b) and compound **1** (Figure 2f) revealed that indeed the primary binding

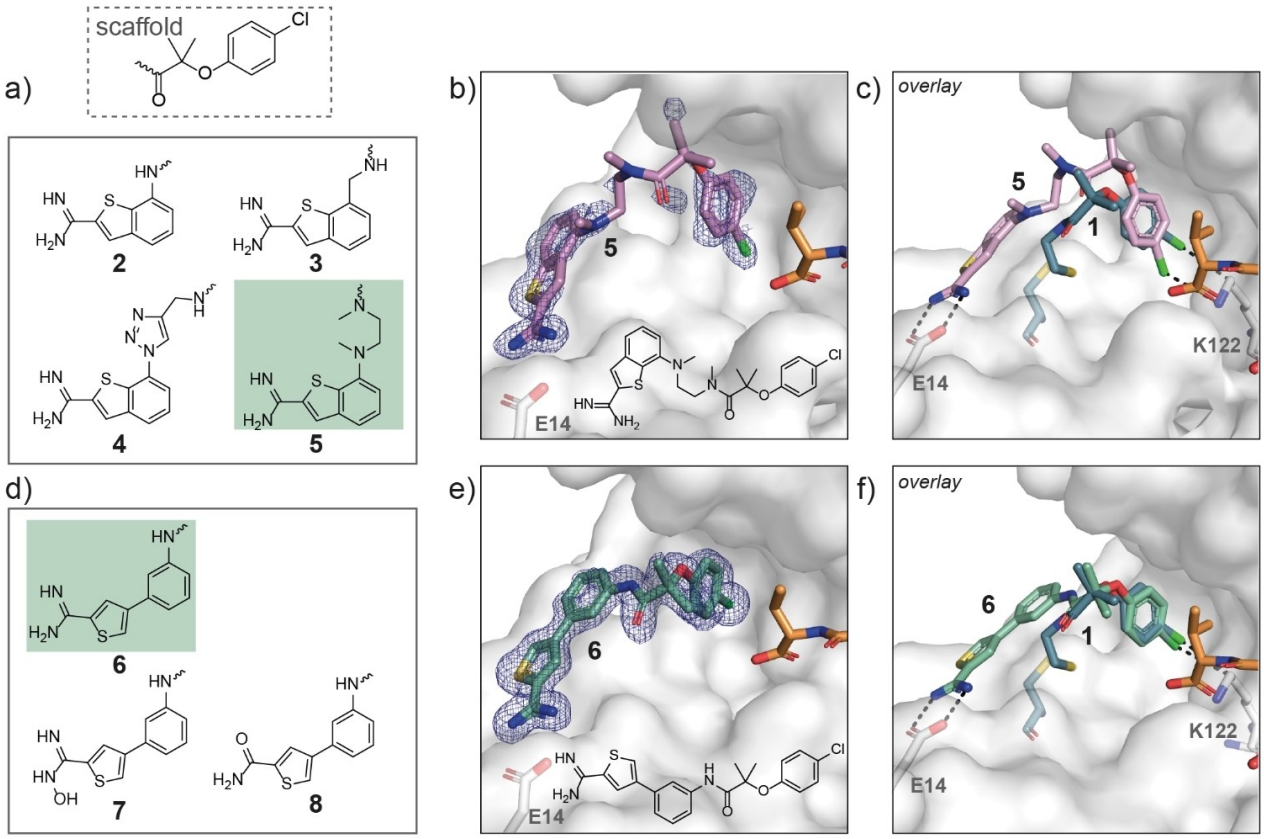

Figure 2. Discovery of first linked fragments. a) Molecular structures of the different linker lengths of benzothiophene building blocks. b) X-ray crystal structure of **5** (pink sticks) in complex with 14-3-3σ (white surface) and ERα phosphopeptide (orange sticks). c) Crystallographic overlay of **5** (pink sticks) with C42-tethered fragment **1** (blue sticks), in complex with 14-3-3σ and ERα phosphopeptide (orange sticks). d) Molecular structures of diphenyl- and phenylthiophene building blocks. e) X-ray crystal structure of **6** (green sticks) in complex with 14-3-3σ (white surface) and ERα phosphopeptide (orange sticks). f) Crystallographic overlay of **6** (green sticks) with C42-tethered fragment **1** (teal sticks), in complex with 14-3-3σ and ERα phosphopeptide (orange sticks).

modes of the original individual fragments were largely conserved in the linked fragment. We therefore synthesized additional analogues of **6** with the aim of improving its stabilization properties. A fluorescence anisotropy (FA) assay was used to analyze the stabilizing properties of the linked fragments. Compounds were titrated in the presence of 14-3-3σ and FAM-labeled ERα phosphopeptide. For stabilizers, a dose-dependent increase in anisotropy was expected. It is noteworthy that for several linked fragments we observed an increase in anisotropy in the absence of 14-3-3, indicative of spectroscopic interference or compound-induced aggregation of the peptide. We crystallized 20 of the synthesized analogues, chemical optimization thus being guided by crystallography. Improved compounds from the series stabilized 14-3-3/ERα binding without significantly interfering with anisotropy in the absence of protein (see below).

We evaluated the structure–activity relationships (SAR) by inspection of the crystal structure of **6** (Figure S6). We hypothesized that a modification of the chlorophenyl moiety was most likely to improve stabilization efficiency because it interacted with both 14-3-3 and the ERα phosphopeptide. The *gem*-dimethyl group made hydrophobic interactions with the side chain of Val595 of ERα as well as Leu218 and Ile219 of 14-3-3. Furthermore, the chlorophenyl moiety was buried in a hydrophobic pocket formed by Phe119, Pro167, Ile168 and Gly171 of 14-3-3 and Val595 of ERα. Based on these observations, we made the following chemical modifications: introducing an amine instead of an ether (Y), changing the chemical nature of the *para* (W) and *meta* (V) substituent on the phenyl ring and, finally, replacing the *gem*-dimethyl group with larger cyclic groups (X; Figure 3a, Table S1).

Exchanging the ether to an amine at position Y (**9**) resulted in a similar binding conformation with a slightly weaker stabilization effect (Figures 3b and S7a). The chlorophenyl moiety buried between the +1 amino acid of the ERα phosphopeptide and 14-3-3 appeared to play an important role for binding of the linked fragment to the protein/peptide complex. When removing this substituent in either the ether (**10**) or the amine variant (**11**) of the hybrid molecules (Figure 3b), the phenyl ring was less anchored resulting in a reduction of electron density (Figure S7b, c). We tested the influence of the substitution of the phenyl ring by changing the chemical nature of the *para* substituent and preparing different combinations of halogen substituents (Figure 3c). Exchanging the chloride with bromide (**12**) or trifluoromethyl (**13**), had no effect on the conformation of the linked fragment nor on that of Lys122 of 14-3-3 (Figure S8a,b). The same held true for an additional halogen decoration in the *meta* position as in **14** (chloro) and **15** (fluoro; Figure 3d, Figure S8c, d).

Deep in the chlorophenyl-accepting pocket, Lys122 was close (4 Å) to the chloride position in **6**, suggesting the possibility of introducing a polar H-bond or buried charge-charge interaction in this otherwise hydrophobic site near the terminal amino group of Lys122. However, exchanging the chloride substituent for an acetyl in **16** resulted in a substantial decline of the quality of the electron density map (Figure 3c, Figure S8e) and did not lead to the engagement of Lys122. Substitution of a methoxy group at the *para* position (**17**) improved electron density (Figure S8f), with the distance of the oxygen atom to the amine of Lys122 being reduced to 3.3 Å. No density was visible for the *para* carboxylic acid group in analogue **18** however.

We next focused on the *gem*-dimethyl (position X) which was in close proximity to a hydrophobic patch in the "roof" of the 14-3-3 channel, including Leu218 and Ile219, and the hydrophobic side chain of Val595 of ERα (Figure S9a). Derivatives with cyclic elaborations of the *gem*-dimethyl moiety were synthesized and soaked into crystals of the 14-3-3σ/ERα phosphopeptide complex (Figure 3e). Four-, five-, and six-membered rings (**19**–**21**, respectively) were well tolerated and produced high-occupancy crystal structures with clear density for the entirety of the molecules (Figure S9b–d).

In addition to the cycloalkyl rings, three compounds were synthesized bearing heterocycles, including a tetrahydropyran (**22**) and piperidine (**23**), or a 4-aminocyclohexyl group (**24**) at position X (Figure 3e). All three compounds showed complete electron density coverage (Figure S10); however, the aminocyclohexyl group in **24** seemed to be less well-defined. Importantly, these compounds did not exhibit an undesirable increase in anisotropy in control experiments lacking 14-3-3, but showed clear 14-3-3/ERα phosphopeptide stabilization (Figure 3h). The addition of solubilizing either or amine functionality at position X (**22**–**24**) might thus have enhanced solubility and decreased aggregation potential. The aniline (Y=N) variant **25**, bearing a piperidine ring as in ether **24**, showed a similar stabilization efficiency and electron density (Figures 3f–h, and S10). A more detailed analysis of the binding modes revealed that the introduction of a hydrogen bond acceptor (**22**) or donor (**23**, **24**, **25**) in the cyclic group X allowed for participation in a network of water molecules, thereby enabling water-mediated interactions with the terminal carboxyl group of Val595 or the carbonyl oxygen of ERα (Figure 3i). These introduced polar interactions thus facilitated interactions with both 14-3-3 and ERα, likely leading to the stabilization observed in FA.

Surprisingly, removal of the *para*-chloro substituent in the context of unsubstituted cyclohexyl (**26**), 4,4-difluorocyclohexane (**27**) or tetrahydropyran ring analogue (**28**; Figure 3g) resulted in a new binding mode wherein the alicyclic or heterocyclic rings replaced the unsubstituted benzene in the interface pocket between 14-3-3 and peptide (Figure S11a–c). In the case of the 4,4-difluorocyclohexane analogue, even the re-introduction of the chloro-substituent (**29**) did not revert the binding mode (Figure S11d), perhaps highlighting the strong preference for halogen decorations for this interface pocket. Additionally, this switch in binding mode caused three other structural effects: I) In the case of the cyclohexyl (**26**) and the difluorocyclohexyl (**27**) compounds, density was observed for an alternative conformation of Val595 of ERα, pointing towards the compound (Figure S11a, b). This effect is also observed for natural product FC-A,[45] where it was proposed to be a favorable conformation for stabilization.

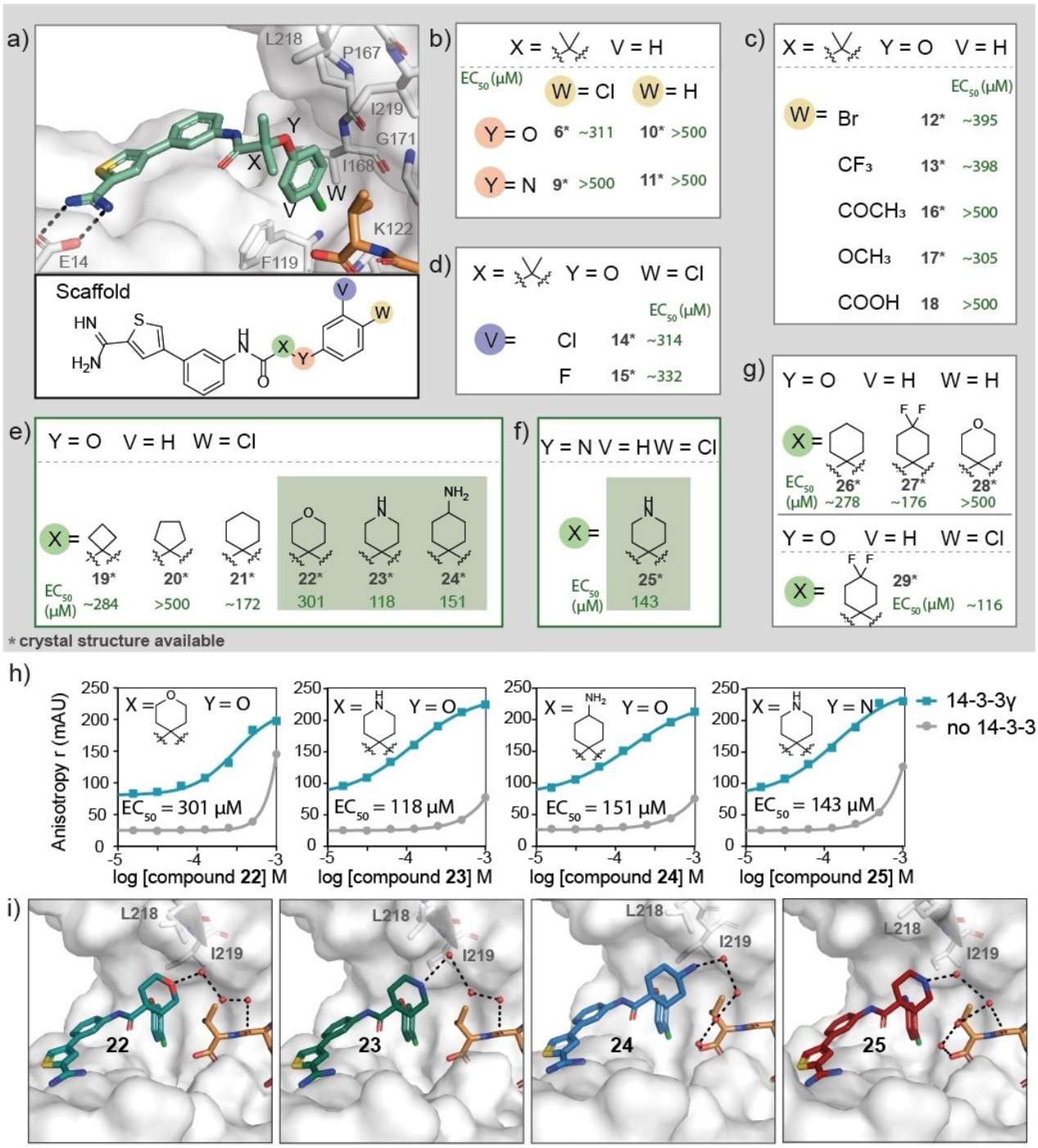

Figure 3. Overview SAR optimization of linked fragments. a–g) Molecular structures of linked fragments with compound ID number (**6**–**29**) and EC_{50} values (μM; green text). If the control (no 14-3-3 protein) also shows an increase in anisotropy, the EC_{50} value is indicated with a ~ sign. An asterisk (*) indicates that the molecule was crystallized. a) Scaffold highlighting positions that were altered at X, Y, V and W. b) Molecules with an ether (Y=O) or an aniline (Y=N) at position Y, with and without a chlorophenyl at position W. c) Molecules with different substituents on the *para* position of the phenyl ring (position W). d) Molecules with different substituents on the *meta* position of the phenyl ring (position V) e) Substitution of larger cyclic groups at the *gem*-dimethyl position (position X). EC_{50} value of active compounds in green box. f) Molecule with piperidine substitution at position X, and an aniline at position Y. EC_{50} value given in green box. g) Molecules synthesized with cyclic substitutions at position X, with or without a chlorophenyl substitution at position W. h) Fluorescence anisotropy (FA) dose-response curves for the linked fragments with a cyclic group at position X containing a hydrogen bond donor or acceptor. Compounds are titrated into FAM-labeled ERα phosphopeptide (10 nM; grey dots) or to a mixture of FAM-labeled ERα phosphopeptide (10 nM) and 14-3-3γ (1 μM; blue squares). i) X-ray crystal structures of **22** (cyan sticks), **23** (green sticks), **24** (marine sticks), and **25** (red sticks), in complex with 14-3-3σ (white surface) and ERα phosphopeptide (orange sticks). Hydrogen bonds are visualized by black dashes and water molecules as red spheres.

II) The phenyl ether oxygen and aniline nitrogen atoms, being displaced from the deeper pocket, were now able to participate in the water network, allowing for water-mediated H-bonds with the C-terminal carboxyl group of ERα (Figure S11e). III) The difluoro group of **27** interacted directly with Lys122 of 14-3-3 and the carboxy group of ERα, with a distance of 3.2 Å and 2.8 Å, respectively (Figure S11f). Compounds **26** and **27**, by virtue of the alternate binding mode they adopt, can be viewed as a second, orthogonal, chemical scaffold for the discovery of more potent stabilizers of ERα and 14-3-3.

We further evaluated the most potent analogues (**23**, **24**, and **25**; EC_{50} values 118 μM, 151 μM, and 143 μM, respectively) though FA 2D-protein titrations (Figure 4a). 14-3-3γ was titrated to FAM-labeled ERα phosphopeptide (10 nM) in the presence of varied concentrations of each compound, resulting in a 21-fold, 25-fold and 15-fold maximum increase in PPI stabilization at 500 μM of **23**, **24** and **25**, respectively. The most potent stabilizer, **24**, was evaluated for its selectivity versus ten representative 14-3-3 client-derived phosphopeptide motifs (Figure 4b). These motifs were selected based on their distinct binding sequences. Compound titrations showed a high selectivity for ERα, which can be explained by the structural overlay of **24** with each peptide client (Figure S12), showing steric clashes with almost all other peptides.

In summary, the stabilization of the 14-3-3/ERα interface by small-molecule linked fragments as described herein is driven by a number of polar and hydrophobic contacts, as exemplified by the complex structure of compound **24** (Figure 4c). The most prominent polar interaction is the salt bridge between the amidine moiety of compound **24** and the side chain of Glu14 in 14-3-3. Furthermore, water-mediated contacts between the amidine of compound **24** and Glu39 and Ser45 of 14-3-3 and the water network involving Glu115 and Asp215 are established by the carbonyl oxygen and the linker nitrogen and oxygen atoms of **24**. At the site of the ERα interface, the 4-amino group of the cyclohexyl ring interacts with a water network involving the backbone of 14-3-3 and the carboxyl terminus of ERα. Important hydrophobic interactions are mediated by the cyclohexyl ring and the side chains of Val595 of ERα as well as Leu218 and Ile219 of 14-3-3σ. The *p*-chlorophenyl moiety is buried in a hydrophobic pocket formed by Phe119, Pro167, Ile168 and Gly171 of 14-3-3 and Val595 of ERα phosphopeptide. Finally, the coplanar phenyl and thiophene rings rest on the terminal amide pi surface, and side-chain methylene of Asn42.

Conclusion

Here we have demonstrated the potential of fragment linking for the development of novel PPI stabilizers, or molecular glues. Our approach utilized one tethered fragment and one reversibly bound, noncovalent fragment as well as crystallography of the quaternary complex including both fragments, 14-3-3, and ERα phosphopeptide. The proximity and positioning of fragments, as revealed in the quaternary structure, allowed for a linker design that conserved the orientations of the individual fragments at the 14-3-3/ERα interface. These initial linked compounds were rapidly developed into more potent and selective stabilizers of the 14-3-3/ERα interaction, making this approach very attractive for the rational design of PPI stabilizers for 14-3-3 PPIs and beyond. We further speculate that fragment linking may be generally more successful when initiated from a tethered fragment as the starting point. Since the tether to cysteine introduces its own constraints on fragment binding, tethering-based screens may intrinsically identify fragment-protein interactions that are more tolerant of non-idealized geometries and distances. This in turn may make their linking to adjacent noncovalent fragments more forgiving of a less-than-perfect linker. Clearly, further optimization of these fragments to higher potency and additional studies involving different and more diverse targets, as well as full-length proteins,[46] will be required to further validate this intriguing notion.

Acknowledgements

The research was supported by funding from the Netherlands Organization of Scientific Research (NWO) through Gravity program 024.001.035 and ECHO grant 711.018.003. Funding was also provided by GM147696, the ONO Pharma Foundation and DFG (CRC1093 program). We thank Dyana Kenanova for critical reading of this manuscript. We acknowledge DESY (Hamburg, Germany), a member of the Helmholtz Association HGF, for the provision of experimental facilities. Parts of this research were carried out at PETRA III, and we would like to thank Sofiane Saouane and Anja Burkhardt for their assistance in using beam P11. Beamtime was allocated for proposals 11008325, 11009075, and 11002907. Further, we acknowledge the European Synchrotron Radiation Facility (ESRF) for the provision of synchrotron radiation facilities, and we would like to thank Matthew Bowler and Gianluca Santoni for assistance and support in using beamline ID30A and ID23-1 (mx2268). The authors also thank Diamond Light Source (DLS) for beamtime (proposal mx-19800-43), and the staff of beamline I03 for assistance with crystal testing and data collection.

Conflict of Interest

Michelle Arkin, Luc Brunsveld and Christian Ottmann are co-founders of Ambagon Therapeutics. Eline Sijbesma and Christian Ottmann are currently employees of Ambagon Therapeutics.

Data Availability Statement

The data that support the findings of this study are available in the supplementary material of this article.

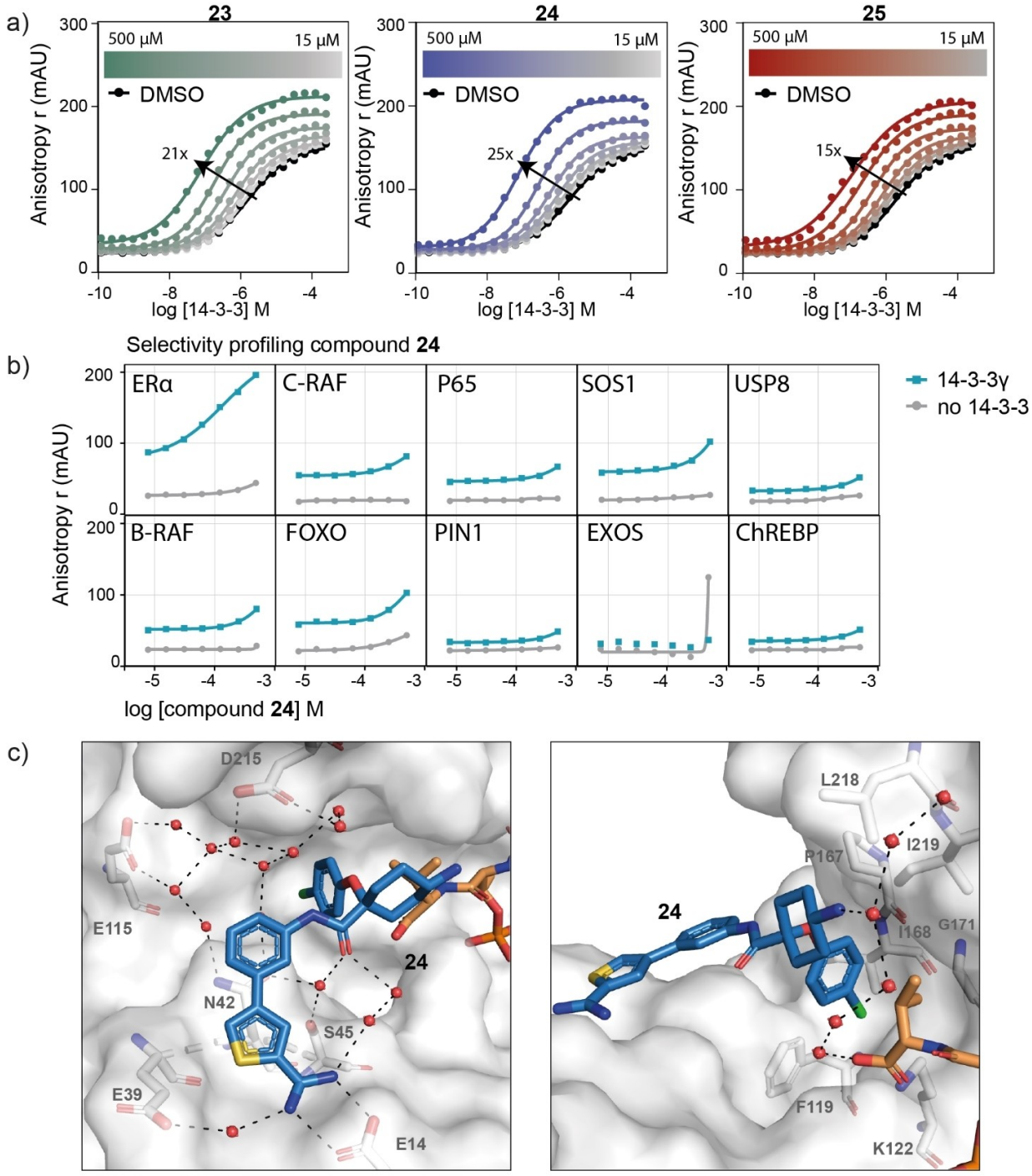

Figure 4. Characterization of stabilizing linked fragments. a) FA 2D titrations with titration of 14-3-3γ to FAM-labeled ERα phosphopeptide (10 nM) against varying concentrations of **23**, **24**, or **25** (ranging from 0 to 500 µM). b) FA with multiple doses of **24** added to ten different client peptides (10 nM each; grey dots), or a mixture containing the peptide and 14-3-3γ (blue squares). c) X-ray crystal structure of **24** (marine sticks) in complex with 14-3-3σ (white surface) and ERα phosphopeptide (orange sticks). Polar interactions are visualized as black dashes and water molecules as red spheres.

Keywords: Drug Discovery · Fragment Linking · Fragment-Based Drug Discovery · Molecular Glues · Proteins

[1] C. J. Gerry, S. L. Schreiber, *Nat. Chem. Biol.* **2020**, *16*, 369–378.
[2] D. A. Nalawansha, C. M. Crews, *Cell Chem. Biol.* **2020**, *27*, 998–1014.
[3] C. Maniaci, A. Ciulli, *Curr. Opin. Chem. Biol.* **2019**, *52*, 145–156.

[4] S. A. Andrei, E. Sijbesma, M. Hann, J. Davis, G. O'Mahony, M. W. D. Perry, A. Karawajczyk, J. Eickhoff, L. Brunsveld, R. G. Doveston, L. G. Milroy, C. Ottmann, *Expert Opin. Drug Discovery* **2017**, *12*, 925–940.

[5] C. Johnson, S. Crowther, M. J. Stafford, D. G. Campbell, R. Toth, C. MacKintosh, *Biochem. J.* **2010**, *427*, 69–78.

[6] E. Park, S. Rawson, K. Li, B. W. Kim, S. B. Ficarro, G. G. Del Pino, H. Sharif, J. A. Marto, H. Jeon, M. J. Eck, *Nature* **2019**, *575*, 545–550.

[7] M. Molzan, S. Kasper, L. Röglin, M. Skwarczynska, T. Sassa, T. Inoue, F. Breitenbuecher, J. Ohkanda, N. Kato, M. Schuler, C. Ottmann, *ACS Chem. Biol.* **2013**, *8*, 1869–1875.

[8] Y. Kondo, S. Banerjee, D. Karandur, A. Merk, K. Kulhanek, K. Wong, J. P. Roose, S. Subramaniam, J. Kuriyan, *Science* **2019**, *366*, 109–115.

[9] S. Rajagopalan, R. S. Sade, F. M. Townsley, A. R. Fersht, *Nucleic Acids Res.* **2010**, *38*, 893–906.

[10] B. Schumacher, J. Mondry, P. Thiel, M. Weyand, C. Ottmann, *FEBS Lett.* **2010**, *584*, 1443–1448.

[11] A. Kuusk, J. F. Neves, K. Bravo-Rodriguez, A. Gunnarsson, Y. B. Ruiz-Blanco, M. Ehrmann, H. Chen, I. Landrieu, E. Sanchez-Garcia, H. Boyd, C. Ottmann, R. G. Doveston, *ACS Chem. Biol.* **2020**, *15*, 262–271.

[12] A. Kuusk, H. Boyd, H. Chen, C. Ottmann, *Biol. Chem.* **2020**, *401*, 921–931.

[13] Y. Joo, B. Schumacher, I. Landrieu, M. Bartel, C. Smet-Nocca, A. Jang, H. S. Choi, N. L. Jeon, K. A. Chang, H. S. Kim, C. Ottmann, Y. H. Suh, *FASEB J.* **2015**, *29*, 4133–4144.

[14] H. Y. Qureshi, T. Li, R. MacDonald, C. M. Cho, N. Leclerc, H. K. Paudel, *Biochemistry* **2013**, *52*, 6445–6455.

[15] S. A. Andrei, F. A. Meijer, J. F. Neves, L. Brunsveld, I. Landrieu, C. Ottmann, L. G. Milroy, *ACS Chem. Neurosci.* **2018**, *9*, 2639–2654.

[16] K. Muda, D. Bertinetti, F. Gesellchen, J. S. Hermann, F. Von Zweydorf, A. Geerlof, A. Jacob, M. Ueffing, C. J. Gloeckner, F. W. Herberg, *Proc. Natl. Acad. Sci. USA* **2014**, *111*, E34–43.

[17] L. M. Stevers, R. M. J. M. de Vries, R. G. Doveston, L.-G. Milroy, L. Brunsveld, C. Ottmann, *Biochem. J.* **2017**, *474*, 1273–1287.

[18] C. Aguilera, V. Fernández-Majada, J. Inglés-Esteve, V. Rodilla, A. Bigas, L. Espinosa, *J. Cell Sci.* **2006**, *119*, 3695–3704.

[19] M. Wolter, P. De Vink, J. F. Neves, S. Srdanović, Y. Higuchi, N. Kato, A. Wilson, I. Landrieu, L. Brunsveld, C. Ottmann, *J. Am. Chem. Soc.* **2020**, *142*, 11772–11783.

[20] C. Ottmann, L. Yasmin, M. Weyand, J. L. Veesenmeyer, M. H. Diaz, R. H. Palmer, M. S. Francis, A. R. Hauser, A. Wittinghofer, B. Hallberg, *EMBO J.* **2007**, *26*, 902–913.

[21] T. Karlberg, P. Hornyak, A. F. Pinto, S. Milanova, M. Ebrahimi, M. Lindberg, N. Püllen, A. Nordström, E. Löverli, R. Caraballo, E. V. Wong, K. Näreoja, A. G. Thorsell, M. Elofsson, E. M. De La Cruz, C. Björkegren, H. Schüler, *Nat. Commun.* **2018**, *9*, 3785.

[22] L. M. Stevers, E. Sijbesma, M. Botta, C. Mackintosh, T. Obsil, I. Landrieu, Y. Cau, A. J. Wilson, A. Karawajczyk, J. Eickhoff, J. Davis, M. Hann, G. O'Mahony, R. G. Doveston, L. Brunsveld, C. Ottmann, *J. Med. Chem.* **2018**, *61*, 3755–3778.

[23] A. M. Hartman, A. K. H. Hirsch, *Eur. J. Med. Chem.* **2017**, *136*, 573–584.

[24] D. Bier, M. Bartel, K. Sies, S. Halbach, Y. Higuchi, Y. Haranosono, T. Brummer, N. Kato, C. Ottmann, *ChemMedChem* **2016**, *11*, 911–918.

[25] C. Anders, Y. Higuchi, K. Koschinsky, M. Bartel, B. Schumacher, P. Thiel, H. Nitta, R. Preisig-Müller, G. Schlichthörl, V. Renigunta, J. Ohkanda, J. Daut, N. Kato, C. Ottmann, *Chem. Biol.* **2013**, *20*, 583–593.

[26] S. A. Andrei, P. de Vink, E. Sijbesma, L. Han, L. Brunsveld, N. Kato, C. Ottmann, Y. Higuchi, *Angew. Chem. Int. Ed.* **2018**, *57*, 13470–13474.

[27] D. Bier, S. Mittal, K. Bravo-Rodriguez, A. Sowislok, X. Guillory, J. Briels, C. Heid, M. Bartel, B. Wettig, L. Brunsveld, E. Sanchez-Garcia, T. Schrader, C. Ottmann, *J. Am. Chem. Soc.* **2017**, *139*, 16256–16263.

[28] F. Bosica, S. A. Andrei, J. F. Neves, P. Brandt, A. Gunnarsson, I. Landrieu, C. Ottmann, G. O'Mahony, *Chem. Eur. J.* **2020**, *26*, 7131–7139.

[29] E. Sijbesma, E. Visser, K. Plitzko, P. Thiel, L. G. Milroy, M. Kaiser, L. Brunsveld, C. Ottmann, *Nat. Commun.* **2020**, *11*, 3954.

[30] E. Sijbesma, K. K. Hallenbeck, S. Leysen, P. J. De Vink, L. Skóra, W. Jahnke, L. Brunsveld, M. R. Arkin, C. Ottmann, *J. Am. Chem. Soc.* **2019**, *141*, 3524–3531.

[31] M. Wolter, D. Valenti, P. J. Cossar, L. M. Levy, S. Hristeva, T. Genski, T. Hoffmann, L. Brunsveld, D. Tzalis, C. Ottmann, *Angew. Chem.* **2020**, *59*, 21520–21524.

[32] E. Sijbesma, B. A. Somsen, G. P. Miley, I. A. Leijten-Van De Gevel, L. Brunsveld, M. R. Arkin, C. Ottmann, *ACS Chem. Biol.* **2020**, *15*, 3143–3148.

[33] X. Guillory, M. Wolter, S. Leysen, J. F. Neves, A. Kuusk, S. Genet, B. Somsen, J. K. Morrow, E. Rivers, L. Van Beek, J. Patel, R. Goodnow, H. Schoenherr, N. Fuller, Q. Cao, R. G. Doveston, L. Brunsveld, M. R. Arkin, P. Castaldi, H. Boyd, I. Landrieu, H. Chen, C. Ottmann, *J. Med. Chem.* **2020**, *63*, 6694–6707.

[34] G. Bollag, P. Hirth, J. Tsai, J. Zhang, P. N. Ibrahim, H. Cho, W. Spevak, C. Zhang, Y. Zhang, G. Habets, E. A. Burton, B. Wong, G. Tsang, B. L. West, B. Powell, R. Shellooe, A. Marimuthu, H. Nguyen, K. Y. J. Zhang, D. R. Artis, J. Schlessinger, F. Su, B. Higgins, R. Iyer, K. Dandrea, A. Koehler, M. Stumm, P. S. Lin, R. J. Lee, J. Grippo, I. Puzanov, K. B. Kim, A. Ribas, G. A. McArthur, J. A. Sosman, P. B. Chapman, K. T. Flaherty, X. Xu, K. L. Nathanson, K. Nolop, *Nature* **2010**, *467*, 596–599.

[35] E. D. Deeks, *Drugs* **2016**, *76*, 979–987.

[36] S. B. Shuker, P. J. Hajduk, R. P. Meadows, S. W. Fesik, *Science* **1996**, *274*, 1531–1534.

[37] P. J. Hajduk, *Mol. Interv.* **2006**, *6*, 266–272.

[38] B. Lamoree, R. E. Hubbard, *Essays Biochem.* **2017**, *61*, 453–464.

[39] H. S. Yu, K. Modugula, O. Ichihara, K. Kramschuster, S. Keng, R. Abel, L. Wang, *J. Chem. Theory Comput.* **2021**, *17*, 450–462.

[40] D. A. Erlanson, S. W. Fesik, R. E. Hubbard, W. Jahnke, H. Jhoti, *Nat. Rev. Drug Discovery* **2016**, *15*, 605–619.

[41] L. R. de Souza Neto, J. T. Moreira-Filho, B. J. Neves, R. L. B. R. Maidana, A. C. R. Guimarães, N. Furnham, C. H. Andrade, F. P. Silva, *Front. Chem.* **2020**, *8*, 93.

[42] P. J. Hajduk, G. Sheppard, D. G. Nettesheim, E. T. Olejniczak, S. B. Shuker, R. P. Meadows, D. H. Steinman, G. M. Carrera, P. A. Marcotte, J. Severin, K. Walter, H. Smith, E. Gubbins, R. Simmer, T. F. Holzman, D. W. Morgan, S. K. Davidsen, J. B. Summers, S. W. Fesik, *J. Am. Chem. Soc.* **1997**, *119*, 5818–5827.

[43] T. Oltersdorf, S. W. Elmore, A. R. Shoemaker, R. C. Armstrong, D. J. Augeri, B. A. Belli, M. Bruncko, T. L. Deckwerth, J. Dinges, P. J. Hajduk, M. K. Joseph, S. Kitada, S. J. Korsmeyer, A. R. Kunzer, A. Letai, C. Li, M. J. Mitten, D. G. Nettesheim, S. C. Ng, P. M. Nimmer, J. M. O'Connor, A. Oleksijew, A. M. Petros, J. C. Reed, W. Shen, S. K. Tahir, C. B. Thompson, K. J. Tomaselli, B. Wang, M. D. Wendt, H. Zhang, S. W. Fesik, S. H. Rosenberg, *Nature* **2005**, *435*, 677–681.

[44] J. Murray, A. M. Giannetti, M. Steffek, P. Gibbons, B. R. Hearn, F. Cohen, C. Tam, C. Pozniak, B. Bravo, J. Lewcock, P. Jaishankar, C. Q. Ly, X. Zhao, Y. Tang, P. Chugha, M. R.

Arkin, J. Flygare, A. R. Renslo, *ChemMedChem* **2014**, *9*, 73–77.

[45] I. J. De Vries-van Leeuwen, D. da Costa Pereira, K. D. Flach, S. R. Piersma, C. Haase, D. Bier, Z. Yalcin, R. Michalides, K. A. Feenstra, C. R. Jimenez, T. F. A. de Greef, L. Brunsveld, C. Ottmann, W. Zwart, A. H. de Boer, *Proc. Natl. Acad. Sci. USA* **2013**, *110*, 8894–8899.

[46] B. A. Somsen, E. Sijbesma, S. Leysen, K. Honzejkova, E. J. Visser, P. J. Cossar, T. Obšil, L. Brunsveld, C. Ottmann, *J. Biol. Chem.* **2023**, *299*, 104855.

Manuscript received: June 7, 2023
Accepted manuscript online: July 16, 2023
Version of record online: August 1, 2023